





Article

# Microstructure and Mechanical Behavior of Hot Extruded Aluminum/Tin-Bismuth Composites Produced by Powder Metallurgy

Adnan Khan <sup>1,†</sup>, Penchal Reddy Matli <sup>2,†</sup>, Muddasir Nawaz <sup>1</sup>, Manohar Reddy Mattli <sup>1</sup>, Gururaj Parande <sup>2</sup>, Vyasaraj Manakari <sup>2</sup>, Abdul Shakoor <sup>1,\*</sup>, Amina Sultan Aljaber <sup>3</sup> and Manoj Gupta <sup>2</sup>

<sup>1</sup> Center for Advanced Materials (CAM), Qatar University, Doha 2713, Qatar; ak1704740@qu.edu.qa (A.K.); m.nawaz@qu.edu.qa (M.N.); m.mattli@qu.edu.qa (M.R.M.)

<sup>2</sup> Department of Mechanical Engineering, National University of Singapore, Singapore 117576, Singapore; drlpenchal@nus.edu.sg (P.R.M.); gururaj.parande@u.nus.edu (G.P.); mbvyasaraj@u.nus.edu (V.M.); mpegm@nus.edu.sg (M.G.)

<sup>3</sup> Department of Chemistry, College of Arts and Science, Qatar University, Doha 2713, Qatar; a.s.aljaber@qu.edu.qa

\* Correspondence: shakoor@qu.edu.qa; Tel.: +974-44036867

† These authors contributed equally to this work.

Received: 13 February 2020; Accepted: 7 April 2020; Published: 18 April 2020



**Abstract:** In this study, Al-BiSn composites were synthesized by a combination of microwave sintering and hot extrusion processes. The structural, morphological, mechanical, and thermal properties were investigated to elucidate the role of Bi<sub>60</sub>Sn<sub>40</sub> (BiSn) alloy content (5, 10, and 15 wt.%) in modifying the properties of Al-BiSn composites. The X-ray diffraction (XRD) patterns confirmed the presence of aluminum and BiSn particles. Distribution of BiSn particles in Al-BiSn composites was confirmed by field emission scanning electron microscopy associated with energy dispersive X-ray analysis (FE-SEM-EDX). Results indicated that hot extruded Al-(15 wt.% BiSn) composite exhibits maximum hardness ( $78 \pm 4$  Hv) and tensile strength ( $185 \pm 3$  MPa), which were 117% and 58% improvements, respectively, compared to pure Al. This improvement in mechanical properties can be attributed to the strengthening effect of BiSn particles. A decline in the values of the coefficient of thermal expansion (CTE) with an increasing amount of BiSn particles reflects the enhanced thermal stability of developed Al-BiSn composites. The promising properties of Al-BiSn composites make them suitable for many industrial applications.

**Keywords:** aluminum; tin-bismuth; composite; powder metallurgy; hot extrusion; mechanical properties

## 1. Introduction

Over the past decades, the demand for lightweight materials with superior mechanical properties has gained significant attention from researchers around the world [1–3]. A wide range of research is focused on developing lightweight materials because of their superior properties when compared to conventional materials [4–7]. Among various composite materials, metal matrix composite (MMC) has gained a lot of attention in automobile [8,9], defense, marine, and aerospace sectors [10,11]. Aluminum metal matrix composites (AMMCs) are known for their high performance and have attracted the attention of most industries due to their provocative properties such as higher strength-to-weight ratio, high hardness, good wear resistance, low density, and decent resistance to corrosion [12–14]. These inviting properties make them attractive for a wide variety of applications. Recently, the application of AMMCs has surged in the above-mentioned sectors, which require high

strength-to-weight ratio, low density, high elastic modulus, excellent thermal stability, and wear resistance. For this purpose, many AMMCs have been developed using various reinforcements, such as alumina ( $\text{Al}_2\text{O}_3$ ) [15], silicon carbide (SiC) [16], boron nitride (BN) [17], titanium carbide (TiC) [18], silicon nitride ( $\text{Si}_3\text{N}_4$ ) [19], boron carbide ( $\text{B}_4\text{C}$ ) [20], Al-Cu-Li [21], nitinol (NiTi) [22], aluminum nitride (AlN) [23], zirconium dioxide ( $\text{ZrO}_2$ ) [24], cerium dioxide ( $\text{CeO}_2$ ) [25], and titanium dioxide ( $\text{TiO}_2$ ) [26], that have shown distinctive contributions in enhancing the structural, thermal, damping, mechanical, and corrosion properties of AMMCs [27,28]. However, there are some limitations in choosing the type of preparation method. Powder metallurgy, forging and stir casting methods are the popular manufacturing techniques to synthesize AMMCs [29–33]. Among these, powder metallurgy (PM) is a simple and cost-effective synthesis technique and provides better results when compared to other processes [34]. Furthermore, PM along with hybrid microwave sintering (HMWS) is suitable for the development of Al-based composites, because it can control the growth in particle size and the changes in microstructure and the volume fraction between the reinforcement and matrix [15–22]. Our research group has reinforced  $\text{Al}_2\text{O}_3$ , TiC,  $\text{Si}_3\text{N}_4$ ,  $\text{B}_4\text{C}$ , BN, and SiC successfully to develop Al-based nanocomposites through the PM technique along with HMWS process.

Tin-bismuth (BiSn) alloy exhibits high strength and hardness, low melting point, superior creep resistance, low thermal expansion coefficient, and low cost, which enables it to be a preferable reinforcement to enhance the mechanical properties of monolithic materials [35]. BiSn composites have been developed by various techniques demonstrating improved properties, such as electrochemical deposition process [36], ball milling with low-temperature melting [37], directional solidification [38], and hydrolysis process [39]; however, there is no reported attempt to use BiSn reinforcement to synthesize aluminum/tin-bismuth (Al-BiSn) composites using microwave-assisted PM technique followed by hot extrusion process. Therefore, the present work focuses on the development of Al-BiSn composites using HMWS technique followed by the hot extrusion process. The structural, mechanical, and thermal properties of the developed Al-BiSn composites with various weight percentages of BiSn particles were investigated.

## 2. Materials and Methods

### 2.1. Synthesis of Al-BiSn Composites

In this study, commercial aluminum (Al) powders (size  $\sim 45 \mu\text{m}$  and purity  $> 99.7\%$ ) were employed as the matrix material.  $\text{Bi}_{60}\text{Sn}_{40}$  (BiSn) alloy particles (average particle size ranging from  $\sim 10\text{--}20 \mu\text{m}$  and purity  $> 99\%$ , supplied by Phoenix Scientific Industries, UK) was added as a reinforcement particle to develop Al-BiSn composites. The scanning electron microscopy (SEM) images and energy dispersive spectroscopy (EDS) spectra of as-received Al and BiSn powder are presented in Figure 1.

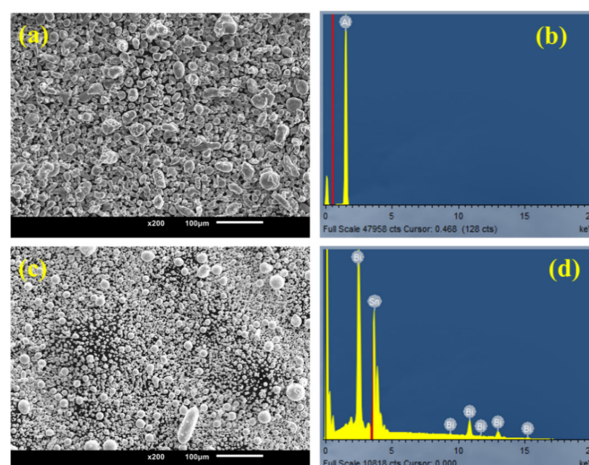


**Figure 1.** SEM images and EDS spectra of (a,b) Al and (c,d) BiSn particles.

A schematic of the experimental process to synthesize Al-BiSn composites is depicted in Figure 2. Pure Al and (5, 10, and 15 wt.%) BiSn-reinforced aluminum composites were synthesized using the PM technique assisted by HMWS. Required amounts of pure Al powder and BiSn particles were carefully weighed and blended for 1 h at 200 rpm in a RETSCH PM-400 mechanical alloying machine (Haan, Germany). No balls or process control agent were used during the blending step, and the blending process was carried out without any protective atmosphere. The blended powder mixtures were then uniaxially cold-compacted at a pressure of 1000 psi to obtain billets of 40 mm in length and 36 mm in diameter. The same parameters were used to compact the pure aluminium without blending. Hybrid microwave-assisted two-directional sintering technology was used to sinter the cold-compacted billets. The billets were heated to 550 °C in a 900 W, 2.45 GHz Sharp microwave oven with SiC as the microwave susceptor material in the absence of an inert atmosphere. The sintering temperature was determined using dummy aluminium blocks and a K-type thermometer in the microwave sintering furnace. A calibration chart (time versus temperature) was made. The compacted billet was sintered in the microwave oven for a precalibrated duration corresponding to a temperature of 550 °C. Following the predetermined time in the microwave, the billet was allowed to cool to room temperature without any holding time under ambient atmospheric conditions. The microwaves were absorbed internally by the billet, and the SiC susceptor heated up to provide radiant heat to the billet externally. This helped in delivering bidirectional heating to the billet as compared to conventional sintering or sintering with microwaves only [40–43]. The as-sintered billet was then further processed using hot extrusion.

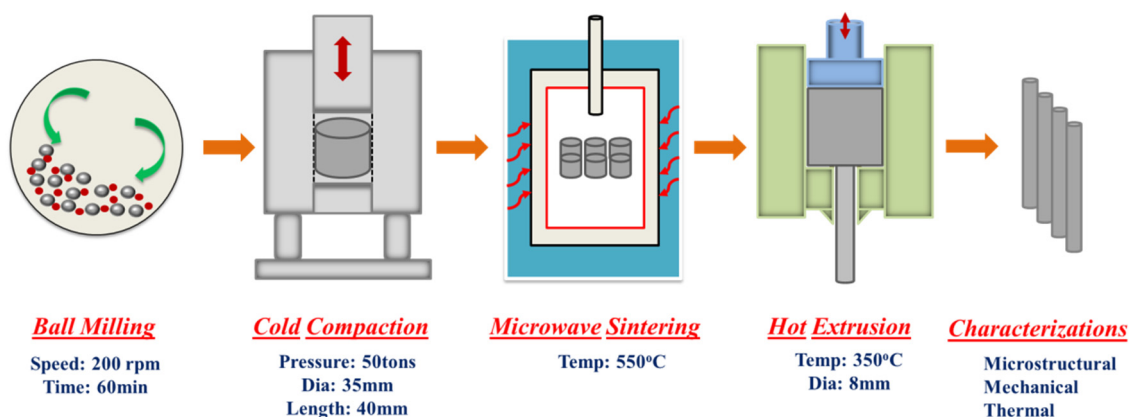


**Figure 2.** The schematic diagram for the synthesis of Al-BiSn composites.

## 2.2. Secondary Processing

Before proceeding towards the hot extrusion process, the microwave sintered billets of pure Al and Al-BiSn composites were soaked at 400 °C for 1 h. Hot extrusion then took place at 350 °C at the extrusion ratio of 20.25:1 using a 150 t hydraulic press to produce 8 mm diameter rods.

## 2.3. Characterization of the Extruded Al-BiSn Composites

Density measurements of the extruded Al and Al-BiSn composites were made following Archimedes' principle on five samples using an electronic balance (A&D ER-182A) with an accuracy of  $\pm 0.0001$  g.

Phase analysis of the pure Al and composites was carried out by X-ray diffraction (XRD) analysis using a PANalytical X'pert Pro diffractometer. The samples were exposed to  $\text{CuK}\alpha$  radiation ( $\lambda = 1.54056 \text{ \AA}$ ) at a scanning rate of  $1.5^\circ/\text{min}$ , in the range of  $20\text{--}90^\circ$  and step size of  $0.02^\circ$ .

The microstructural analyses were carried out on small sections of the extruded rod, which were cut with a diamond blade and smoothed using SiC papers to remove all the visible scratches. The microstructures were studied using a field emission scanning electron microscope (FE-SEM, S-4300, Hitachi, Japan), equipped with an energy dispersive spectroscopy (EDS) detector. The surface

morphology of the Al-BiSn composites was studied using an atomic force microscope (AFM, MFP-3D Nanoindenter).

The microhardness tests were performed using a Vickers indenter tester (FM-ARS9000, USA) following the ASTM standards E384–99 (load of 50 gf and a dwell time of 15 s). In order to ensure the accuracy and repeatability of the results, fifteen readings were taken per individual sample. Nanoindentation analysis was performed using an MFP-3D Nano Indenter (head connected to AFM equipment) equipped with standard Berkovich diamond indenter tip. The testing was performed at room temperature. The indentation was conducted at a maximum load of 100 mN under loading/unloading rate of 200  $\mu\text{N/s}$ , providing dwell time of 5 s at the maximum load.

Tensile tests of pure Al and Al-BiSn composite samples were carried out according to ASTM E8/E8M-15a on the universal testing machine (Lloyd-Ametek LR50K Plus) at room temperature at a strain rate of  $8.3 \times 10^{-4} \text{ s}^{-1}$ . For each composition, five tests were performed to obtain the average and repeatable values. From the load–displacement curves, 0.2% offset yield strength (YS), ultimate tensile strength (UTS), and elongation (ductility) were determined.

The coefficients of thermal expansion (CTE) of extruded Al and its composites were measured through the thermo-mechanical analyzer (INSEIS TMA PT 1000LT). A heating rate of 5  $^{\circ}\text{C}/\text{min}$  for a temperature range of 50–350  $^{\circ}\text{C}$  with an argon flow rate of 0.1 liters per minute was used during the experiment.

### 3. Results and Discussion

#### 3.1. Density and Porosity of Al-BiSn Composites

Figure 3 depicts the measured density and porosity of extruded pure Al and Al-BiSn composites with different BiSn contents. The average measured density values of the extruded Al-BiSn composites increase with the incremental BiSn content due to the high density of BiSn alloy (8.12–8.56  $\text{g}/\text{cm}^3$ ) which is almost 3 times that of pure Al (2.70  $\text{g}/\text{cm}^3$ ). Further, with an increasing amount of BiSn in Al-BiSn composites, the percentage of porosity also increased. This increment in the porosity can be regarded as the pronounced effect of particle agglomeration due to the high amount of reinforcement and pore nucleation between the Al matrix and BiSn interfaces. These findings are consistent with previous studies [15,21].

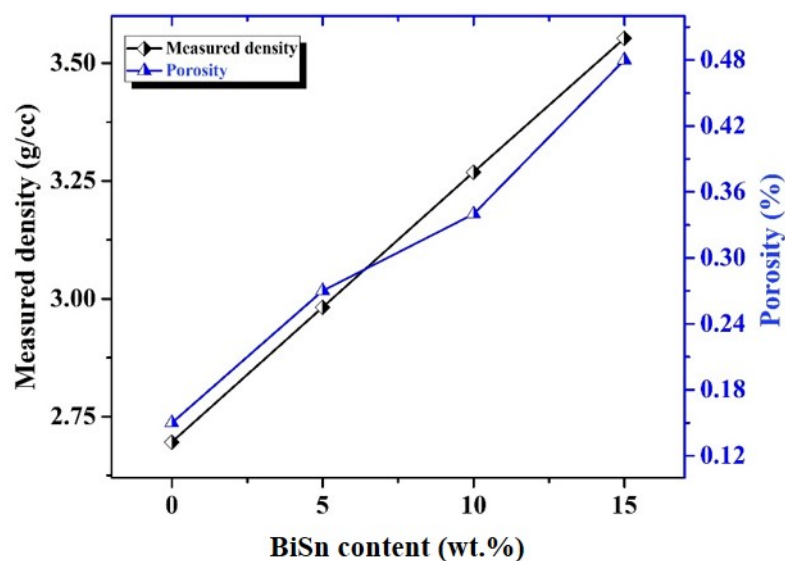


**Figure 3.** The fluctuation of measured density and porosity of Al-BiSn composites as a function of BiSn content.

### 3.2. XRD Analysis of Al-BiSn Composites

XRD patterns of all extruded and polished samples were analyzed. Figure 4 shows the XRD results of extruded Al and Al-BiSn composites containing various concentrations (5, 10, and 15 wt.%) of BiSn. In pure Al, characteristic peaks of (111), (200), (220), (311), and (222) are noticed, representing a typical face-centered cubic structure (FCC) of Al. Moreover, it is also noticed that in Al-BiSn composites containing 5 wt.% of BiSn, the peaks of the reinforcements are not visible. This may be due to either the low concentration of BiSn in the composite, which is below the detectable limit of the XRD machine, or to the high relative intensity of peaks of crystalline Al.

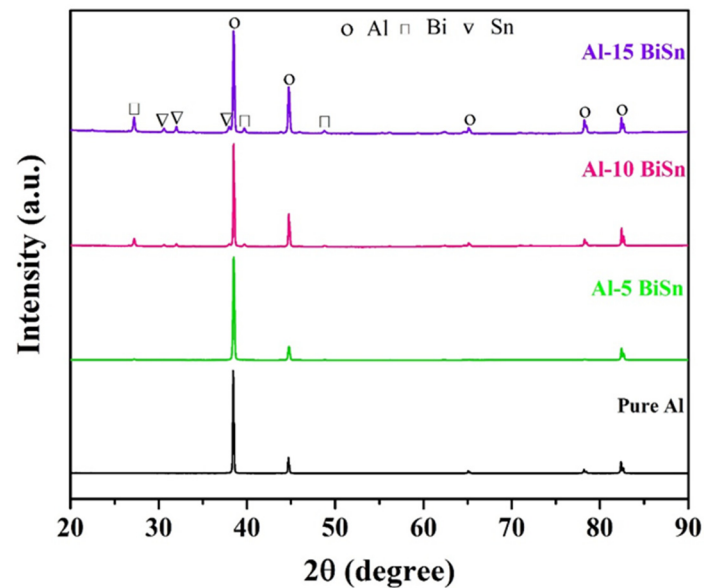


**Figure 4.** X-ray diffraction patterns of extruded Al-BiSn composites.

### 3.3. Field Emission Scanning Electron Microscopy Analysis of Al-BiSn Composites

Figure 5a–d represents the field emission scanning electron microscopy (FE-SEM) micrographs which reveal the morphology of the extruded Al-BiSn (0–15 wt.%) composites. In pure Al, a clear dark matrix with no reinforcement is observed (Figure 5a). A homogeneous distribution of the BiSn particles (indicated by arrow marks) in Al matrix is noticed for all Al-BiSn composites (Figure 5b–d). Moreover, good interfacial integrity of the bright BiSn particles in the dark Al matrix also confirms the incorporation of BiSn in Al matrix. It is pertinent to mention here that a partial agglomeration of the BiSn particles is also observed in the developed Al-(15 wt.% BiSn) composites. The energy dispersive X-ray (EDX) analysis of Al-BiSn composites containing 10 and 15 wt.% BiSn is presented in Figure 5e,f, which confirms the existence of BiSn particles in Al matrix.

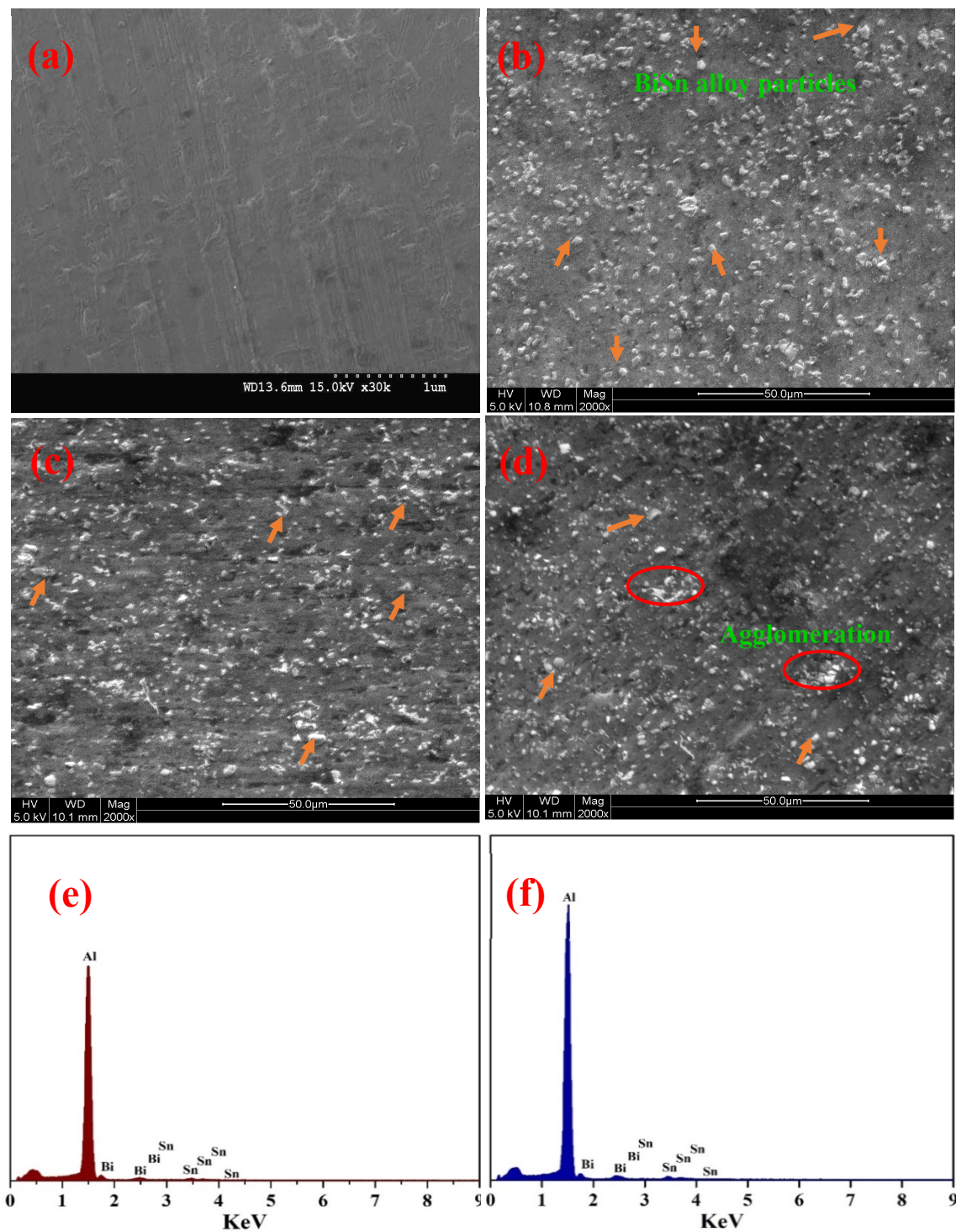


**Figure 5.** FE-SEM images of (a) pure Al and (b) Al-(5 wt.% BiSn), (c) Al-(10 wt.% BiSn), and (d) Al-(15 wt.% BiSn) extruded composites. (e,f) EDX analysis of Al-BiSn composites with 10 and 15 wt.% of BiSn.

### 3.4. Atomic Force Microscopy Analysis of Al-BiSn Composites

Atomic force microscopy (AFM) was carried out to examine the surface morphology of the extruded Al-BiSn composites. The AFM images of the extruded Al-BiSn composites containing different BiSn contents are represented in Figure 6a–d. The root-mean-square (RMS) roughness has been used to describe the surface roughness of the developed composites. The extruded pure Al sample,

having a single homogeneous grain of Al, has resulted in a very smooth surface (RMS = 16.68 nm). However, the surface roughness of Al-BiSn composites increases with the increasing amount of BiSn content, reaching 20.26 nm at the optimum concentration (15 wt.% of BiSn). This increase in surface roughness can be attributed to (i) the incremental increase in the micron-sized BiSn particles in the Al matrix, (ii) the new interface of the reinforcement, and (iii) the high clustering/agglomeration of the BiSn particles, which was also noted in the FE-SEM images (Figure 5b–d).

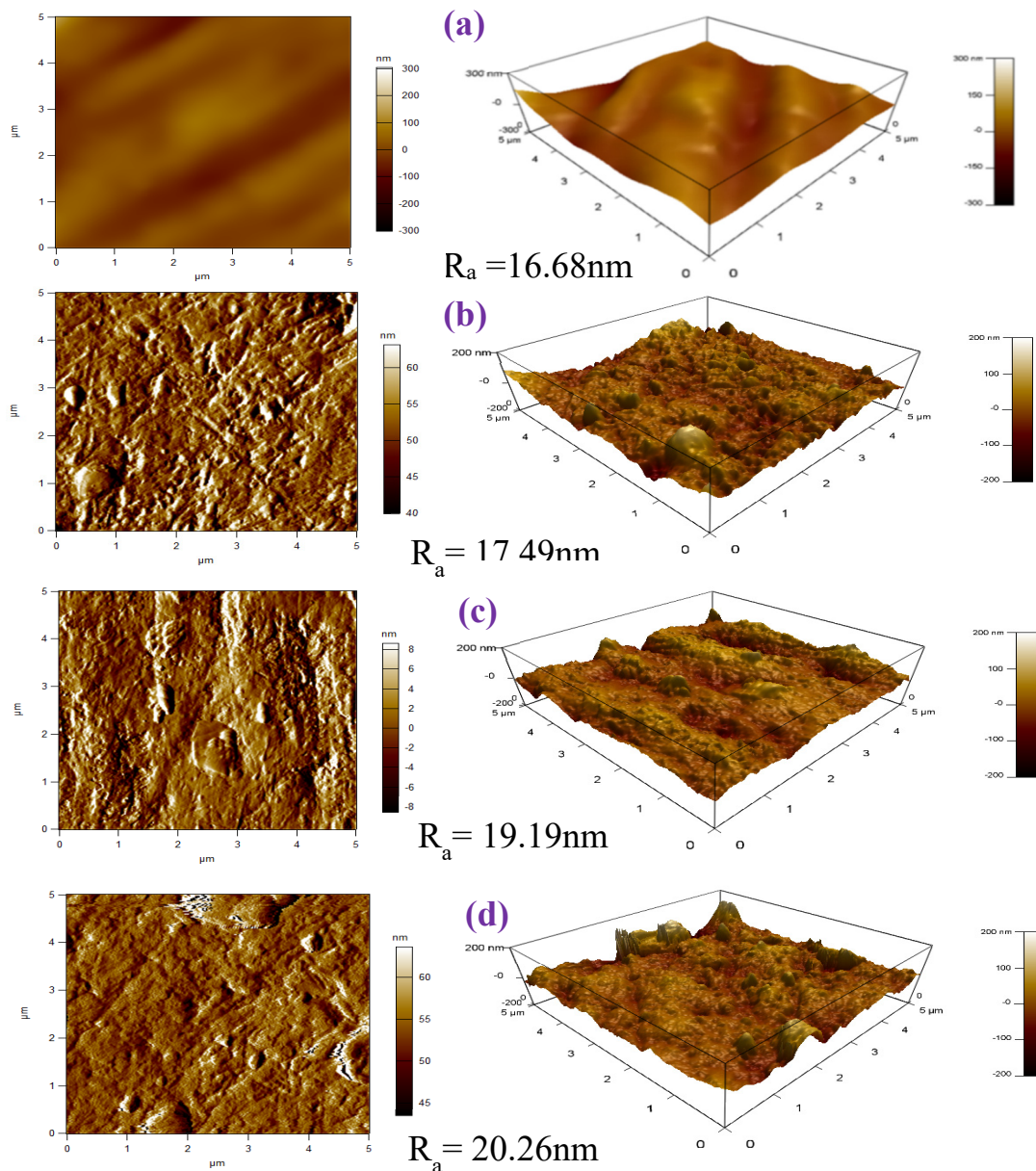


**Figure 6.** Two-dimensional and three-dimensional AFM micrographs of (a) pure Al and (b) Al-(5 wt.% BiSn), (c) Al-(10 wt.% BiSn), and (d) Al-(15 wt.% BiSn) extruded composites.

### 3.5. Microhardness and Nanoindentation Analysis of Al-BiSn Composites

The microhardness variation of the Al-BiSn composites with BiSn amount is shown in Figure 7a. The microhardness of the extruded Al-BiSn composites increases with the increasing BiSn content. The hardness increases from  $36 \pm 2$  (pure Al) to  $78 \pm 4$  HV (15 wt.% of BiSn), indicating an increment of 117%. The increasing trend of the hardness in Al-BiSn composites with an increasing amount of BiSn reflects the efficient and uniform dispersion of BiSn particles in the Al matrix. This improvement in

hardness with increasing concentration of BiSn particles can also be ascribed to the strengthening effects of BiSn reinforcement. Furthermore, near-dense materials synthesized with the powder metallurgy method, microwave sintering, and hot extrusion may have also contributed to enhancing the hardness of the developed Al-BiSn composites.

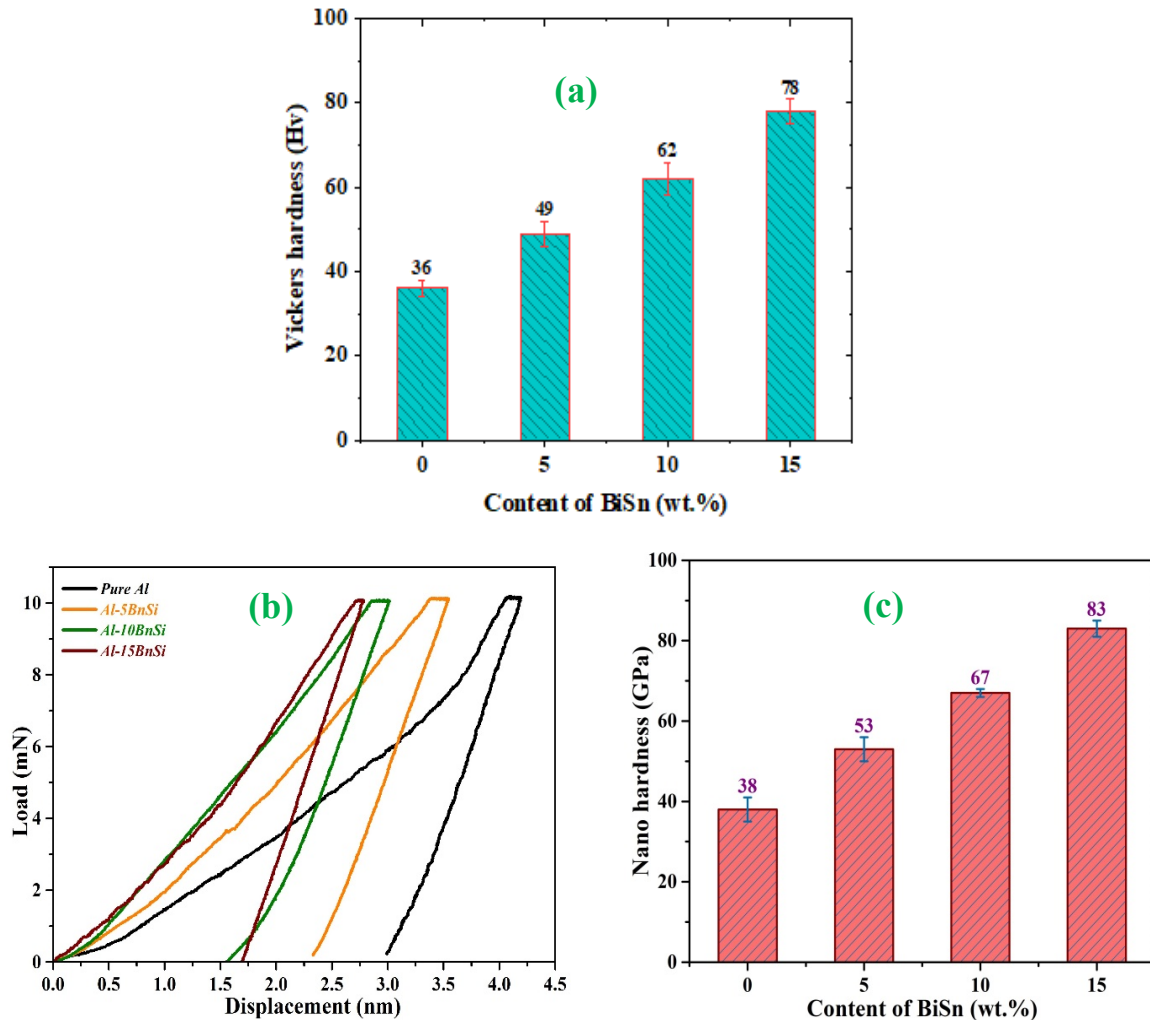


**Figure 7.** The variation of Vickers hardness with BiSn content (a) and nanoindentation results (b,c) of pure Al and Al-BiSn composites.

Nanoindentation analysis of extruded Al-BiSn composites was further conducted to have more insight into the mechanical behavior of the developed composites. The load–displacement curves are presented in Figure 7b. A lower depth of penetration is noted for the developed Al-BiSn composites when compared to pure Al. Moreover, the depth of penetration decreases with the increasing amount of BiSn particles, suggesting an increase in hardness with an increasing amount of reinforcement (Figure 7c). The increase in the hardness and decrease in the indentation depth with the increasing BiSn volume fraction show that hard BiSn particles are homogeneously dispersed in the Al matrix and offer a hindering effect to the indenter. The highest resistance offered to penetration is  $83 \pm 2$  GPa for Al-BiSn composites containing 15 wt.% BiSn. The nanoindentation results of Al-BiSn composites are in line with their Vickers hardness results.

### 3.6. Tensile Properties of Al-BiSn Composites

Figure 8a presents the stress–strain curves of the extruded Al-BiSn composites carried out at room temperature under tensile loading. The corresponding variation of yield strength and ultimate tensile



strength with different volume fractions of BiSn is presented in Figure 8b. Table 1 lists the detailed data of the tensile properties. A significant improvement in the yield strength (YS) and the ultimate tensile strength (UTS) is noted with an increasing amount (5, 10, and 15 wt.%) of BiSn particles in the Al matrix. The Al-(15 wt.% BiSn) composite exhibited significantly higher ultimate tensile strength ( $185 \pm 3$  MPa) and yield strength ( $164 \pm 5$  MPa), which are enhanced by 58% and 78%, respectively, when compared to pure Al. This improvement in mechanical properties of the developed composites can be ascribed to (i) the homogeneous mixing of the BiSn particles in Al matrix, (ii) the hindering of the dislocation motion by BiSn particles, and (iii) the efficient load transfer because of the strong bond of the BiSn particle to the Al matrix. These findings are consistent with the previous studies [15,21]. The uniform dispersion and strong bonding of the reinforcement (BiSn) to the Al matrix are evident from FE-SEM images (Figure 5b–d). It can be observed that, with the addition of BiSn reinforcement, the strength is noticeably increased without compromising ductility. These results are consistent with similar studies using BN and B<sub>4</sub>C particles as reinforcement [17,20]. In Table 1, the developed Al-BiSn composites are also compared with the already published Al-based composites [15,21,44–47].

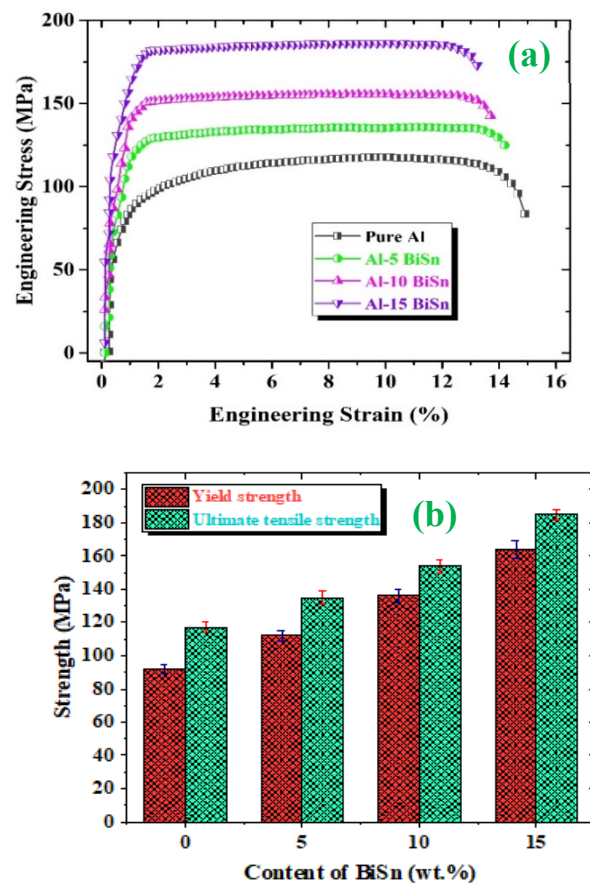


**Figure 8.** (a) Tensile stress–strain curves of extruded Al-BiSn composites and (b) variation of yield strength (YS) and ultimate tensile strength (UTS) of the extruded composites with different amounts of BiSn.

**Table 1.** Comparison of the hardness and tensile properties of Al-BiSn composites with other studies.

Material	Hardness		Tensile Properties		
	Micro (HV)	Nano (GPa)	Yield Strength/MPa	Ultimate Tensile Strength/MPa	% of Elongation
Pure Al	36 ± 2	38 ± 3	92 ± 3	117 ± 3	13.70
Al-(5 wt.% BiSn)	49 ± 6	53 ± 4	112 ± 3	135 ± 4	13.45
Al-(10 wt.% BiSn)	62 ± 4	67 ± 1	136 ± 4	154 ± 1	12.76
Al-(15 wt.% BiSn)	78 ± 4	83 ± 2	164 ± 5	185 ± 3	12.04
Al-(10 wt.% Al <sub>2</sub> O <sub>3</sub> ) [15]	73 ± 6	-	118 ± 5	141 ± 5	9.4 ± 0.5
Al-(10 wt.% AlCuLi) [21]	72 ± 3	-	122 ± 3	152 ± 6	8.3 ± 0.5
Al-(3 wt.% SiC) [44]	56.1	-	142	162	4.7
Al-(3 wt.% SiO <sub>2</sub> ) [45]	38.7	-	100	137	0.9
Al-(5 wt.% GNP) [46]	-	-	22	27	0.2
Al-(10 wt.% TiO <sub>2</sub> ) [47]	37	-	64	76	5.33

### 3.7. Fracture Analysis of the Al-BiSn Composites

Fractography observations were conducted to understand the fracture mechanisms of the tensile-tested samples. Figure 9a–d shows the fracture surfaces of the extruded pure Al and Al-BiSn composites containing 5, 10, and 15 wt.% of BiSn particles. The presence of fine dimples in the fractured surfaces represents the ductile mode of fracture. This feature represents the ductile and high plastic deforming nature of the Al-BiSn composites. The similar nature of the fracture in all compositions of the Al-BiSn composites suggests that the fracture behavior of the Al-BiSn composite is mainly dependent on the deformation behavior of the Al matrix. As a comparison, a larger number of dimples with smaller size are noted in Al-BiSn composites, explaining the high UTS of Al-BiSn composites.

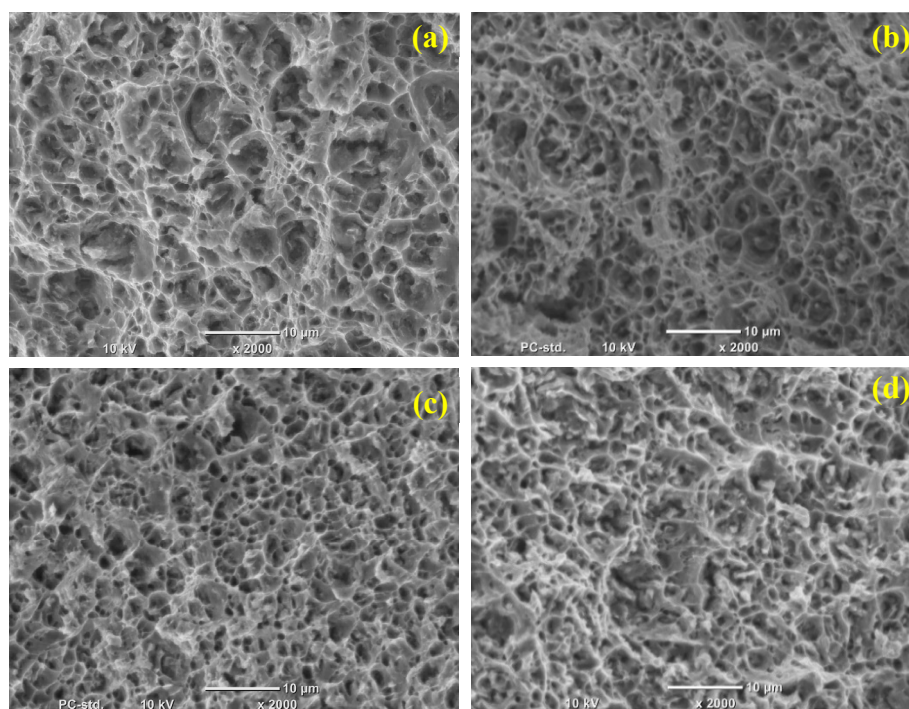


**Figure 9.** Fractography studied materials under tensile mode: (a) pure Al and (b) Al-(5 wt.% BiSn), (c) Al-(10 wt.% BiSn), and (d) Al-(15 wt.% BiSn) composites.

### 3.8. Coefficient of Thermal Expansion (CTE) of Al-BiSn Composites

The variation in the coefficient of thermal expansion (CTE) values of extruded Al-BiSn composites with BiSn content is presented in Figure 10. A decline in the CTE values is observed with an increasing amount of BiSn, reflecting improved thermal stability of the developed Al-BiSn composites.

The measured CTE value of the pure Al observed is  $\sim 23.31 \mu/k$ , which is very close to the theoretical CTE value of Al. By adding 5 wt.% of BiSn in Al, the CTE value decreases to  $\sim 22.14 \mu/k$ , which reflects an enhanced constraint on the thermal expansion by the additional interface of BiSn. Further increase in BiSn content leads to further decrease in the CTE values, reaching  $\sim 19.86 \mu/k$  at 15 wt.% of BiSn. In comparison with pure Al, the continuous decrease of the CTE values with the increasing amount of BiSn particles confirms enhanced thermal stability of the Al-BiSn composites. The behavior of CTE values is similar to the other Al-based composites present in the literature [18,20]. Owing to their low CTE value, the Al-BiSn composites can be regarded as a potential material to be used in aerospace, automobile, and electrical industries.

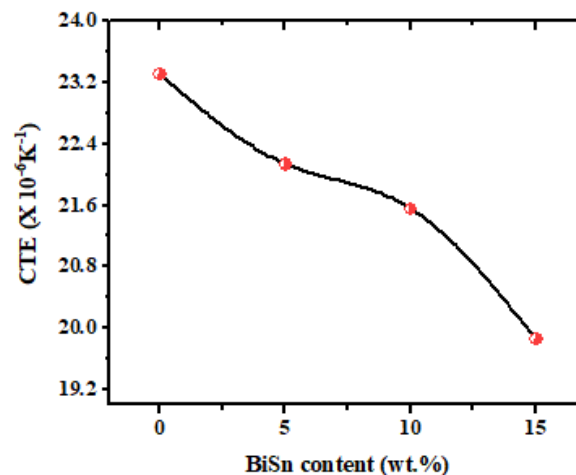


**Figure 10.** The variation of coefficient of thermal expansion (CTE) of extruded Al-BiSn composites as a function of BiSn content.

#### 4. Conclusions

Aluminum composites reinforced with BiSn alloy particles can be developed by microwave-assisted PM followed by the hot extrusion process. The microstructural, mechanical, and thermal performances of Al-BiSn composites were investigated. The FE-SEM microstructures reveal a uniform distribution of BiSn particles in the aluminum matrix. Tensile results showed a 58% increase in the strength, from  $117 \pm 3$  MPa for pure Al to  $185 \pm 3$  MPa for Al-(15 wt.% BiSn) composite. The enhanced mechanical properties are ascribed to the homogeneously distributed BiSn particles and their strengthening effects. The CTE values for the Al-BiSn composites decreased with increasing BiSn content. Good mechanical and thermal properties of Al-BiSn composites make them attractive for aerospace, automobile, defense, and electrical industries. From the synthesis perspective, HMWS has a wide range of potential advantages for developing Al-based nanocomposites because of its rapid heating capability.

**Author Contributions:** A.K. and P.R.M. wrote the main part of the manuscript and developed the planning of the experiment. P.R.M., G.P., and V.M. carried out the preparation of different composite materials and tested thermal properties. M.N., M.R.M., and A.S.A. performed characterization of the microstructure and mechanical studies of the samples. A.S. and M.G. supervised the materials preparation process and commented on the manuscript draft. All authors have read and agreed to the published version of the manuscript.

**Funding:** This research received no external funding.

**Acknowledgments:** The authors greatly acknowledge the technical support of the Center for Advanced Materials (CAM), Qatar University, 2713, Doha, Qatar. The authors would also like to thank the Central laboratory Unit (CLU), Qatar University, for SEM analysis.

**Conflicts of Interest:** The authors declare no conflict of interest.

## References

1. Manakari, V.; Parande, G.; Gupta, M. Selective Laser Melting of Magnesium and Magnesium Alloy Powders: A Review. *Metals* **2016**, *7*, 2. [[CrossRef](#)]
2. Manakari, V.; Parande, G.; Doddamani, M.; Gupta, M. Enhancing the Ignition, Hardness and Compressive Response of Magnesium by Reinforcing with Hollow Glass Microballoons. *Materials* **2017**, *10*, 997. [[CrossRef](#)] [[PubMed](#)]
3. Matli, P.R.; Krishnan, A.V.; Manakari, V.; Parande, G.; Chua, B.; Wong, S.; Lim, C.; Gupta, M. A new method to lightweight and improve strength to weight ratio of magnesium by creating a controlled defect. *J. Mater. Res. Technol.* **2020**. [[CrossRef](#)]
4. Benedyk, J. Aluminum alloys for lightweight automotive structures. In *Materials, Design and Manufacturing for Lightweight Vehicles*; Elsevier BV: Amsterdam, The Netherlands, 2010; pp. 79–113.
5. Subramanian, J.; Seetharaman, S.; Gupta, M. Processing and Properties of Aluminum and Magnesium Based Composites Containing Amorphous Reinforcement: A Review. *Metals* **2015**, *5*, 743–762. [[CrossRef](#)]
6. Parande, G.; Manakari, V.; Koppaarthi, S.D.S.; Gupta, M. A study on the effect of low-cost eggshell reinforcement on the immersion, damping and mechanical properties of magnesium–zinc alloy. *Compos. Part B Eng.* **2020**, *182*, 107650. [[CrossRef](#)]
7. Thornby, J.; Verma, D.; Cochrane, R.; Westwood, A.; Manakari, V.B.; Gupta, M.; Haghshenas, M. Indentation-based characterization of creep and hardness behavior of magnesium carbon nanotube nanocomposites at room temperature. *SN Appl. Sci.* **2019**, *1*, 695. [[CrossRef](#)]
8. Mallick, P. Advanced materials for automotive applications: An overview. In *Advanced Materials in Automotive Engineering*; Elsevier BV: Amsterdam, The Netherlands, 2012; pp. 5–27.
9. Prasad, S.; Asthana, R. Aluminum Metal–Matrix Composites for Automotive Applications: Tribological Considerations. *Tribol. Lett.* **2004**, *17*, 445–453. [[CrossRef](#)]
10. Casati, R.; Vedani, M. Metal Matrix Composites Reinforced by Nano-Particles—A Review. *Metals* **2014**, *4*, 65–83. [[CrossRef](#)]
11. Chawla, K.K. Metal Matrix Composites. In *Composite Materials*; Springer Science and Business Media LLC: New York, NY, USA, 2019; pp. 199–249.
12. Das, D.K.; Mishra, P.C.; Singh, S.; Thakur, R.K. Properties of ceramic-reinforced aluminium matrix composites—A review. *Int. J. Mech. Mater. Eng.* **2014**, *9*, 25. [[CrossRef](#)]
13. Rajak, D.K.; Pagar, D.D.; Kumar, R.; Pruncu, C.I. Recent progress of reinforcement materials: A comprehensive overview of composite materials. *J. Mater. Res. Technol.* **2019**, *8*, 6354–6374. [[CrossRef](#)]
14. Sharma, P.; Sharma, S.; Khanduja, D. A study on microstructure of aluminium matrix composites. *J. Asian Ceram. Soc.* **2015**, *3*, 240–244. [[CrossRef](#)]
15. Reddy, M.P.; Ubaid, F.; Shakoor, R.A.; Parande, G.; Manakari, V.; Mohamed, A.M.A.; Gupta, M. Effect of reinforcement concentration on the properties of hot extruded Al–Al<sub>2</sub>O<sub>3</sub> composites synthesized through microwave sintering process. *Mater. Sci. Eng. A* **2017**, *696*, 60–69. [[CrossRef](#)]
16. Matli, P.; Shakoor, R.; Parande, G.; Manakari, V.; Ubaid, F.; Mohamed, A.; Gupta, M. Enhanced performance of nano-sized SiC reinforced Al metal matrix nanocomposites synthesized through microwave sintering and hot extrusion techniques. *Prog. Nat. Sci.* **2017**, *27*, 606–614.
17. Reddy, M.P.; Manakari, V.; Parande, G.; Ubaid, F.; Shakoor, R.; Mohamed, A.M.A.; Gupta, M. Enhancing compressive, tensile, thermal and damping response of pure Al using BN nanoparticles. *J. Alloy. Compd.* **2018**, *762*, 398–408. [[CrossRef](#)]
18. Reddy, M.P.; Himyan, M.; Ubaid, F.; Shakoor, R.A.; Vyasaraj, M.; Gururaj, P.; Yusuf, M.; Mohamed, A.; Gupta, M. Enhancing thermal and mechanical response of aluminum using nanolength scale TiC ceramic reinforcement. *Ceram. Int.* **2018**, *44*, 9247–9254. [[CrossRef](#)]
19. Matli, P.R.; Ubaid, F.; Shakoor, R.A.; Parande, G.; Manakari, V.; Yusuf, M.; Mohamed, A.M.A.; Gupta, M. Improved properties of Al–Si<sub>3</sub>N<sub>4</sub> nanocomposites fabricated through a microwave sintering and hot extrusion process. *RSC Adv.* **2017**, *7*, 34401–34410. [[CrossRef](#)]
20. Ubaid, F.; Matli, P.R.; Shakoor, R.A.; Parande, G.; Manakari, V.; Mohamed, A.M.A.; Gupta, M. Using B<sub>4</sub>C Nanoparticles to Enhance Thermal and Mechanical Response of Aluminum. *Materials* **2017**, *10*, 621. [[CrossRef](#)]

21. Reddy, M.P.; Manakari, V.; Parande, G.; Shakoor, R.A.; Mohamed, A.M.A.; Gupta, M. Structural, mechanical and thermal characteristics of Al-Cu-Li particle reinforced Al-matrix composites synthesized by microwave sintering and hot extrusion. *Compos. Part B Eng.* **2019**, *164*, 485–492. [[CrossRef](#)]
22. Matli, P.; Manakari, V.; Parande, G.; Mattli, M.; Shakoor, R.A.; Gupta, M. Improving Mechanical, Thermal and Damping Properties of NiTi (Nitinol) Reinforced Aluminum Nanocomposites. *J. Compos. Sci.* **2020**, *4*, 19. [[CrossRef](#)]
23. Cho, S.C.; Han, C.; Choi, H.; Kim, H.S.; Jin, S.; Han, J.H. Synthesis and consolidation behavior of Al/AlN composite powders by reactive RF thermal plasma spraying. *Powder Technol.* **2016**, *287*, 395–402. [[CrossRef](#)]
24. Kumar, G.; Pramod, R.; Sekhar, C.G.; Bhanumurthy, T.; Kumar, G. Investigation of physical, mechanical and tribological properties of Al6061–ZrO<sub>2</sub> nano-composites. *Heliyon* **2019**, *5*, e02858. [[CrossRef](#)] [[PubMed](#)]
25. Mohammed, H.; Reddy, M.P.; Ubaid, F.; Shakoor, R.A.; Mohamed, A.M.A. Structural and mechanical properties of CeO<sub>2</sub> reinforced Al matrix nanocomposites. *Adv. Mater. Lett.* **2018**, *9*, 602–605. [[CrossRef](#)]
26. Oke, S.R.; Falodun, O.E.; Mahlatse, M.R.; Ige, O.O.; Olubambi, P.A. Investigation on densification and microstructure of Al-TiO<sub>2</sub> composite produced by Spark plasma sintering. *Mater. Today Proc.* **2019**, *18*, 3182–3188.
27. Cavaliere, P.; Jahantigh, F.; Shabani, A.; Sadeghi, B. Influence of SiO<sub>2</sub> nanoparticles on the microstructure and mechanical properties of Al matrix nanocomposites fabricated by spark plasma sintering. *Compos. Part B Eng.* **2018**, *146*, 60–68. [[CrossRef](#)]
28. Sharma, P.; Sharma, S.; Khanduja, D. Production and some properties of Si<sub>3</sub>N<sub>4</sub> reinforced aluminium alloy composites. *J. Asian Ceram. Soc.* **2015**, *3*, 352–359. [[CrossRef](#)]
29. Chandra, D.; Chauhan, N.R.; Rajesha, S. *Hardness and Toughness Evaluation of Developed Al Metal Matrix Composite Using Stir Casting Method*; Elsevier BV: Amsterdam, The Netherlands, 2020.
30. Das, J.; Chandra, K.; Misra, P.; Sarma, B. Hardness and tensile properties of Fe–P based alloys made through powder forging technique. *Mater. Sci. Eng. A* **2008**, *479*, 164–170. [[CrossRef](#)]
31. C, G.M.; Hiremath, P.; Shettar, M.; Sharma, S.; U, S.R. Experimental validity on the casting characteristics of stir cast aluminium composites. *J. Mater. Res. Technol.* **2020**. [[CrossRef](#)]
32. Kane, S.N.; Mishra, A.; Gaur, A. PREFACE: International Conference on Recent Trends in Physics (ICRTP 2014). *J. Phys. Conf. Ser.* **2014**. [[CrossRef](#)]
33. Purohit, R.; Qureshi, M.; Kumar, B. Effect of Forging on Aluminum Matrix Nano Composites: A Review. *Mater. Today Proc.* **2017**, *4*, 5357–5360. [[CrossRef](#)]
34. Gessinger, G.H. Recent Developments in Powder Metallurgy. *Met. Sci.* **1974**, *8*, 394–396. [[CrossRef](#)]
35. Abdelaziz, S.M.; Zahran, H.; El-Rehim, A.A. Microstructure and mechanical properties of tin-bismuth solder alloy reinforced by antimony oxide nanoparticles. *Int. J. Adv. Eng. Technol.* **2017**, *10*, 73.
36. Peng, Y.; Deng, K. Fabrication of reduced graphene oxide nanosheets reinforced Sn–Bi nanocomposites by electro-chemical deposition. *Compos. Part A Appl. Sci. Manuf.* **2015**, *73*, 55–62. [[CrossRef](#)]
37. He, P.; Lü, X.-C.; Lin, T.; Li, H.-X.; An, J.; Ma, X.; Feng, J.; Zhang, Y.; Li, Q.; Qian, Y.-Y. Improvement of mechanical properties of Sn–58Bi alloy with multi-walled carbon nanotubes. *Trans. Nonferrous Met. Soc. China* **2012**, *22*, s692–s696. [[CrossRef](#)]
38. Costa, T.; Freitas, E.S.; Dias, M.; Brito, C.; Cheung, N.; Garcia, A. Monotectic Al–Bi–Sn alloys directionally solidified: Effects of Bi content, growth rate and cooling rate on the microstructural evolution and hardness. *J. Alloy. Compd.* **2015**, *653*, 243–254. [[CrossRef](#)]
39. Du Preez, S.P. Hydrogen Generation by Means of Hydrolysis Using Activated Al-In-Bi-Sn Composites for Electrochemical Energy Applications. *Int. J. Electrochem. Sci.* **2017**, 8663–8682. [[CrossRef](#)]
40. Kujur, M.S.; Mallick, A.; Manakari, V.; Parande, G.; Tun, K.S.; Gupta, M. Significantly Enhancing the Ignition/Compression/Damping Response of Monolithic Magnesium by Addition of Sm<sub>2</sub>O<sub>3</sub> Nanoparticles. *Metals* **2017**, *7*, 357. [[CrossRef](#)]
41. Parande, G.; Manakari, V.; Meenashisundaram, G.K.; Gupta, M. Enhancing the tensile and ignition response of monolithic magnesium by reinforcing with silica nanoparticulates. *J. Mater. Res.* **2017**, *32*, 2169–2178. [[CrossRef](#)]
42. Parande, G.; Manakari, V.; Koppaarthi, S.D.S.; Gupta, M. Utilizing Low-Cost Eggshell Particles to Enhance the Mechanical Response of Mg-2.5Zn Magnesium Alloy Matrix. *Adv. Eng. Mater.* **2017**, *20*, 1700919. [[CrossRef](#)]

43. Kujur, M.S.; Manakari, V.; Parande, G.; Tun, K.S.; Mallick, A.; Gupta, M. Enhancement of thermal, mechanical, ignition and damping response of magnesium using nano-ceria particles. *Ceram. Int.* **2018**, *44*, 15035–15043. [[CrossRef](#)]
44. Zeng, X.; Liu, W.; Xu, B.; Shu, G.; Li, Q.-L. Microstructure and Mechanical Properties of Al–SiC Nanocomposites Synthesized by Surface-Modified Aluminium Powder. *Metals* **2018**, *8*, 253. [[CrossRef](#)]
45. Issa, H.K.; Taherizadeh, A.; Maleki, A.; Ghaei, A. Development of an aluminum/amorphous nano-SiO<sub>2</sub> composite using powder metallurgy and hot extrusion processes. *Ceram. Int.* **2017**, *43*, 14582–14592. [[CrossRef](#)]
46. Bisht, A.; Srivastava, M.; Kumar, R.M.; Lahiri, I.; Lahiri, D.; Kumar, M.R. Strengthening mechanism in graphene nanoplatelets reinforced aluminum composite fabricated through spark plasma sintering. *Mater. Sci. Eng. A* **2017**, *695*, 20–28. [[CrossRef](#)]
47. Ravichandran, M.; Meignanamoorthy, M.; Dineshkumar, S. Microstructure and Properties of Hot Extruded Al-TiO<sub>2</sub> Powder Metallurgic Composites. *Appl. Mech. Mater.* **2016**, *852*, 130–135. [[CrossRef](#)]



© 2020 by the authors. Licensee MDPI, Basel, Switzerland. This article is an open access article distributed under the terms and conditions of the Creative Commons Attribution (CC BY) license (<http://creativecommons.org/licenses/by/4.0/>).